

Improved silicon optical parameters at 25°C, 295 K and 300 K including temperature coefficients

Martin A. Green 

Australian Centre for Advanced Photovoltaics,
 School of Photovoltaic and Renewable Energy
 Engineering, University of New South Wales
 (UNSW), Sydney, New South Wales, Australia

Correspondence

Martin A. Green, Australian Centre for
 Advanced Photovoltaics, School of
 Photovoltaic and Renewable Energy
 Engineering, University of New South Wales
 (UNSW), Sydney, NSW 2052, Australia.
 Email: m.green@unsw.edu.au

Funding information

Australian Renewable Energy Agency

Abstract

Although the author's earlier tabulations of silicon's refractive index and absorption coefficient over a wide range of wavelengths have found wide use, recent luminescent measurements have shown that refinement is needed at wavelengths beyond 1200 nm. An updated dataset is described for lightly doped silicon tabulated over the 250- to 1450-nm range in 10-nm increments at three temperatures, 25°C, 295 K and 300 K, incorporating the most recent experimental results. Temperature coefficients are also included allowing reasonably accurate estimates of optical parameters over the much broader –24°C to 200°C range.

KEY WORDS

silicon absorption coefficient, silicon optical properties, silicon refractive index

1 | INTRODUCTION

Since the publication of two earlier datasets,^{1,2} finding wide use within the photovoltaic community, luminescent measurements have provided more stringent testing of the accuracy of those datasets with shortcomings apparent beyond 1200 nm.^{3–6} Deficiencies can be traced to the matching procedure used with the earlier data when combining two independent datasets at 1190 nm. Modifying this matching procedure corrects this difficulty. Additionally, improved experimental data have been published that additionally decrease the uncertainty in published values. Incorporating these developments, fresh tabulations are described with an emphasis on values at 25°C, a temperature relevant to photovoltaic device simulation and performance specification, as well as at 295 K (nominally room temperature) and 300 K, two other frequently used reference temperatures.

2 | DATA SOURCES

Measurements of the silicon absorption coefficient to ultralow values from the spectral response of high-performance solar cells prompted the publishing of an extended dataset of silicon optical properties in 1995 that has found wide use.¹ This dataset was further refined² in 2008 by using a Kramers–Kronig (K-K) analysis of reflection to

combine a diverse range of previously published data over a wide wavelength range. Because absorption at wavelengths beyond 500 nm has little impact on silicon reflection, values at long wavelengths required direct measurement and additionally on the matching procedure mentioned above beyond 1190 nm.

Because the improved spectral response data predated the first sensitive photoluminescence measurements,⁷ no sensitive check upon the matching procedure was possible at the time of original publication.¹ However, careful photoluminescence measurements on high-quality silicon ingots³ in 2012 clearly identified a problem in the matching procedure used, with the published dataset² predicting emission that was too high beyond 1200 nm. Refining the matching procedure to reduce all values at 1190-nm wavelength and beyond by 20% gives good agreement with the experimental luminescence data. The original dataset² with this change will be referred to as ‘Green 2008 revised’ and will be used in lieu of the former throughout this document.

There have been several additional relevant developments^{4–6,8,9} allowing further refinements to be incorporated into the new dataset reported in the present paper. One has been the publishing of an extended absorption coefficient dataset determined by photoluminescence from 78 to 363 K over the 990- to 1300-nm wavelength range by Nguyen et al.⁴; the second, the publishing of a preliminary study by Schinke et al. of 295-K data including carefully

considered uncertainty estimates⁵; and, the third, the publishing of an improved and more comprehensive study by Schinke et al.⁶ again of 295-K data but using a wider range of techniques, forming a complete and consistent absorption dataset over the 250- to 1450-nm range, completely independent from that compiled by Green.² Other significant developments have been the publishing⁸ of extremely accurate values of silicon's refractive index for wavelengths beyond 1100 nm and the measurement of silicon optical properties at short wavelength by techniques other than spectroscopic ellipsometry,⁹ with the latter known to be very sensitive to silicon surface layers.

Using these and additional data sources, the final absorption coefficient dataset of Schinke et al.⁶ at 295 K (nominally room temperature) was refined by detailed comparison with high-quality independent experimental data, reducing the published uncertainty in regions where this was high. This modified dataset was then extrapolated to produce a dataset at the intermediate temperature of 25°C, as most commonly used in solar device simulations and performance specification and also at 300 K, another frequently used reference temperature. These tabulations allow calculation of the imaginary part of the refractive index at these three temperatures. The real part of the refractive index is less sensitive to temperature with values tabulated at 25°C only. Values at the other two reference temperatures differ by less than 1 digit in the third decimal place, with accuracy to the fourth decimal place possible, in situations where such accuracy is required, by combining with the presently published temperature coefficients, also tabulated at 25°C.

3 | TEMPERATURE AND BANDGAP NARROWING EFFECTS

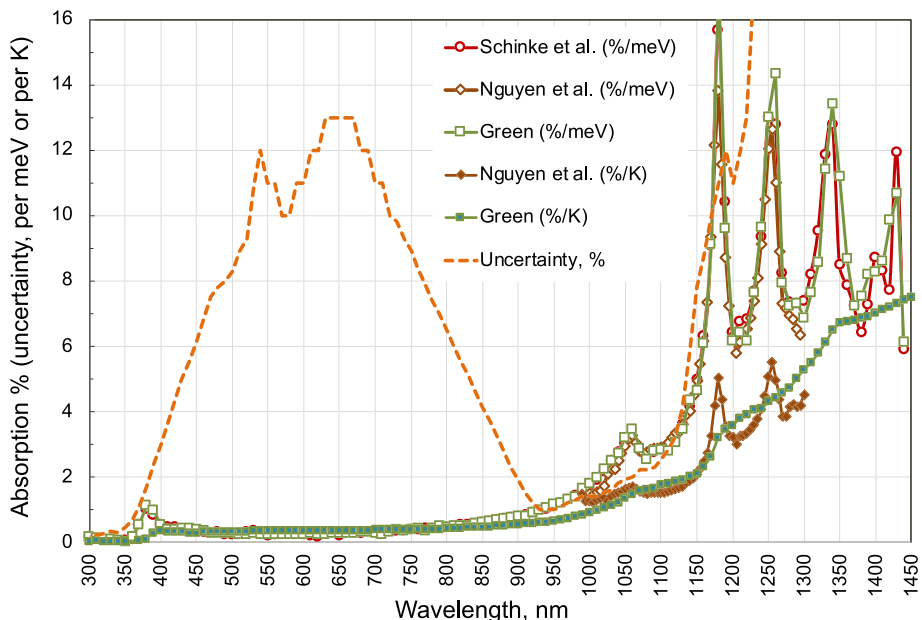
Increasing accuracy in tabulated values means that more attention has to be paid not only to temperature but also to bandgap narrowing

than in previous work. The percentage change in absorption properties introduced by 1°C temperature increase is shown in Figure 1 together with that from a 1-meV increase in photon energy. It can be seen that the two are closely related, as earlier noted by Weakliem and Redfield,¹⁰ who provided a relationship between the two over the 1.1- to 2.5-eV range (500- to 1130-nm range). In essence, this suggests that a 1°C increase in temperature causes the same change in absorption as a 1.2-meV increase in photon energy over the 1.7- to 2.5-eV (500–730 nm) range, with this 1.2-meV value reducing linearly with reducing photon energy over the 1.1- to 1.7-eV range (730–1130 nm) to a value of 0.43 meV at 1.1 eV (1130 nm). Note that a 1°C increase in temperature decreases the indirect bandgap of silicon by 0.27 meV and the direct bandgap by 0.41 meV, contributing the corresponding magnitudes to the above figures, although augmented by additional temperature effects.

Figure 2A shows the ratio of the change due to a 1°C increase in temperature to a 1-meV increase in energy as a function of wavelength, as deduced by Weakliem and Redfield and also as calculated from the datasets of Green 2008 revised and Schinke et al.⁶ All are in reasonable agreement except at short wavelength below 280 nm where the datasets of Green² and Schinke et al.⁶ give strongly divergent results. This disagreement can be resolved by noting that earlier results from both Jellison et al.¹¹ and Vuye et al.¹² specifically studying temperature dependencies show that, for energies in the 4.35- to 5.2-eV range (240–285 nm), the absorption coefficient decreases with increasing energy and also with increasing temperature. This means that the above ratio must be positive, in agreement with Green but not with Schinke et al.⁶ as subsequently discussed.

The strong features particularly apparent in the energy dependence curves of Figure 1 are due to a series of different absorption thresholds (wavelength derivative absorption spectroscopy has long been used to investigate these thresholds). The prominent short-wavelength peak at 380 nm (3.3 eV) is associated with the onset of

FIGURE 1 The sensitivity of the measured value of the 295-K absorption coefficient (in percent) to a 1°C increase in temperature (open markers) or a 1-meV increase in photon energy (closed markers). Also shown is the reported percentage uncertainty ($k = 2$) in the measurements of Schinke et al.,⁶ highlighting regions where meeting the stated uncertainty would require precise temperature control and/or where deduced values may be specific to particular doping or injection levels



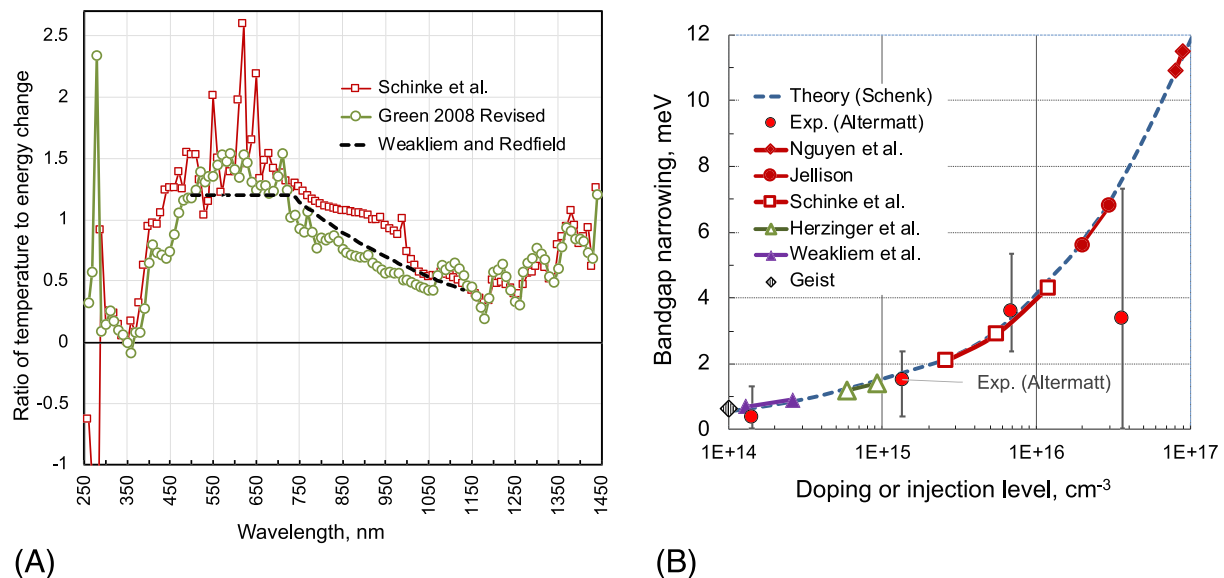


FIGURE 2 (A) The ratio of the change due to a 1°C increase in temperature to a 1-meV increase in photon energy; (B) theoretical bandgap narrowing as a function of doping or injection level as calculated by Schenk¹³ (independent of dopant type in the range shown) together with the experimental support deduced by Altermatt et al.¹⁴ from the work of Sproul and Green.¹⁵ Also shown are the doping or injection levels and the deduced bandgap narrowing for the samples used for some of the key measurements discussed

direct bandgap absorption in silicon, while that at 1060 nm (1.17 eV) is similarly associated with indirect bandgap absorption with emission of a momentum conserving transverse optical (TO) phonon. The next at 1180 nm (1.05 eV) is due to photon absorption accompanied by absorption of this phonon. Those at longer wavelengths involve the absorption of several phonons, largely this momentum conserving TO phonon in combination with one or more zone centre, Raman active phonons.

Below 900 nm, silicon optical constants vary only slowly with temperature, and the practice of citing ‘room temperature’ values, often without specifying the specific temperature involved, is reasonable unless very low error margins are sought (temperature accuracy within a few degrees is adequate at most wavelengths below 900 nm unless accuracy better than 1% is sought). ‘Room temperature’ generally means a temperature in the 20–25°C range, with reportedly only the International Union of Pure and Applied Chemistry defining a specific temperature (25°C) as ‘room temperature’. We will follow Schinke et al.^{5,6} in taking 295 K (~22°C) as representative of ‘room temperature’, given the quality of the data generated by these authors at this temperature.

There are two other comments to make re temperature coefficients. The mathematically correct value is the derivative of the parameter involved with respect to temperature. However, this value may not be as useful as a value representing the average slope over the targeted extrapolation range (little error in small extrapolations using the latter value but potentially much better accuracy for large extrapolations!). This explains some of the differences between the two temperature dependency datasets shown in Figure 1. Additionally, extrapolating with values involving strong features, such as the

phonon absorption features at long wavelengths, may cause undesirable side effects. Accordingly, values previously published by Green² were determined by a procedure, subsequently to be described, that gives smoothed values conducive to long-range extrapolation but, as also pointed out by Nguyen et al.,⁴ are unable to correctly incorporate temperature dependent shifts in absorption thresholds.

Bandgap narrowing effects may not have received the attention warranted in earlier datasets with calculated doping or injection levels dependencies for these shown in Figure 2B. For example, the photoluminescence-based data of Nguyen et al.⁴ were derived using circa 12 suns excitation with the sample in high injection (carrier concentrations were estimated as in the 8–9 × 10¹⁶/cm³ range near room temperature⁴). According to the theoretical work of Schenk,¹³ presently the most highly regarded for silicon photovoltaic device work in this area, this corresponds to bandgap narrowing of over 10 meV near room temperature (Figure 2B), appreciably higher than in other datasets, where samples typically doped in the 1- to 100-Ocm range were used. Because there exists no known way of correcting data for such narrowing across the spectrum, the comprehensive dataset of Nguyen et al.⁴ must be used with caution for present purposes, although useful for investigating temperature dependencies as subsequently discussed.

Due to the lack of such a procedure for spectral correction, the most useful values to tabulate were considered to be values at low to moderate doping levels typical of semiconductor use, such as in photovoltaics and microelectronics. For the present tables, values relevant to doping levels in the 10¹⁵–10¹⁶/cm³ range (or injected concentrations at this level) are targeted rather than values for intrinsic silicon. From Figure 2B, it is apparent that some data lie outside this range,

notably those of Nguyen et al.⁴ at the high end, as already noted. The early but highly regarded data of McFarlane et al.¹⁶ lie at the low end and may not be applicable for more typical doping ranges (the McFarlane et al.¹⁶ data were based on use of ‘high purity’ silicon ingots, interpreted as ingots grown without intentional doping). At long wavelengths where absorption across silicon’s indirect bandgap is the strongest optical process, doping reduces the bandgap increasing absorption at any given wavelength as well as blurring features associated with the onset of each phonon absorption mode (possibly due to optical selection rule relaxation due to the random distribution of dopants), with similar effects from increased injection level. At shorter wavelengths, doping can blur features associated with the direct bandgap transitions near 3.4 eV (E_0' and E_1 critical points, subsequently discussed), actually reducing absorption coefficient values close to 360-nm wavelength and similarly reducing the value of the absorption peak at 280–290 nm (associated with $E_2(X)$ and $E_2(\Sigma)$ critical points).

4 | 295-K ABSORPTION COEFFICIENT DATASET

Readers only interested in final data selection are directed straight to Section 4.5

4.1 | Comparison of recent results

The care taken with uncertainty estimates in the work of Schinke et al.⁶ and its complete independence from other datasets give the opportunity for refinement and generation of a new dataset with reduced uncertainty. A close examination of differences between this dataset and that of Green,² based on a wide variety of sources, allows improvements to both.

Green’s 2008 revised data were extrapolated to 295 K using Green’s published temperature coefficients² with the percentage deviation of the Schinke et al. data from this extrapolated dataset shown in Figure 3. Also shown is the uncertainty estimates provided by Schinke et al.⁶ (coverage factor, $k = 2$, roughly corresponding to 95% confidence that the actual value lies within this range). The two datasets are in agreement within this uncertainty range except in the 250- to 530-nm wavelength and the 1020–1130-nm ranges where the uncertainty in both datasets is reasonably low, implying inconsistent data requiring closer examination. On the other hand, consistency is high in regions where the uncertainty estimates are large, suggesting that combining the two datasets could reduce overall uncertainty in these regions.

4.2 | Short wavelength region (250–500 nm)

The short wavelength region includes the onset of direct bandgap optical transitions along the Σ direction at 4.49 eV (276 nm), near the

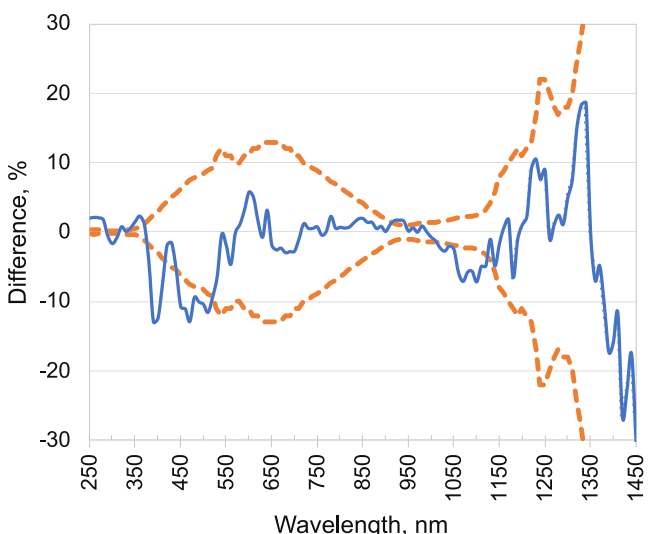


FIGURE 3 Percentage difference between the datasets of Green² (revised) and Schinke et al.⁶ (blue solid line). Also shown are the Schinke et al.⁶ uncertainty estimates (orange dashed lines; coverage factor $k = 2$)

X point ($E_2(X)$ critical point) at 4.27 eV (290 nm), near the L point (E_1 critical point) at 3.38 eV (367 nm) and at zone centre (E_0' critical point) at 3.32 eV (373 nm).¹⁷ These direct transitions are energetically closely spaced, due to roughly parallel conduction and valence bands along multiple k -space directions, making silicon one of the most strongly absorbing semiconductors in this wavelength range. The range also includes the onset of indirect absorption across the second indirect gap (zone centre to L point) at about 2.5 eV (~500 nm) combined with the strong increase in all indirect absorption as the energy deficit in the associated virtual transition approaches zero.¹⁸

Published optical property measurements in this wavelength range are largely dependent on spectroscopic ellipsometry as the measurement technique, known to be highly sensitive to surface layers and surface roughness. K-K reflection analysis as used by Green² is a nominally independent technique, although Green used the detailed tabulation of optical constants deduced from ellipsometry by Herzinger et al.¹⁹ to establish a reflection baseline, likely reducing this independence.

Tabulated room temperature data from various sources are compared with the data of Green² and Schinke et al.⁶ in Figure 4A over the 250- to 300-nm range (encompassing two of the previous critical points). These other data sources include the seminal ellipsometric data of Aspnes and Studna,²⁰ the highly regarded data of Jellison,²¹ the detailed data of Herzinger et al.¹⁹ (where particular care was taken to eliminate surface layer effects) and the most recent data of Humlíček and Šík⁹ intended to resolve inconsistencies in earlier datasets. The consistency between these four datasets over this wavelength range is high with less than 1% deviation between them typical.

The Herzinger et al.¹⁹ data are particularly impressive with the unsmoothed second derivative of the permittivity (real and imaginary) with respect to energy also shown (as deduced by the simplest finite

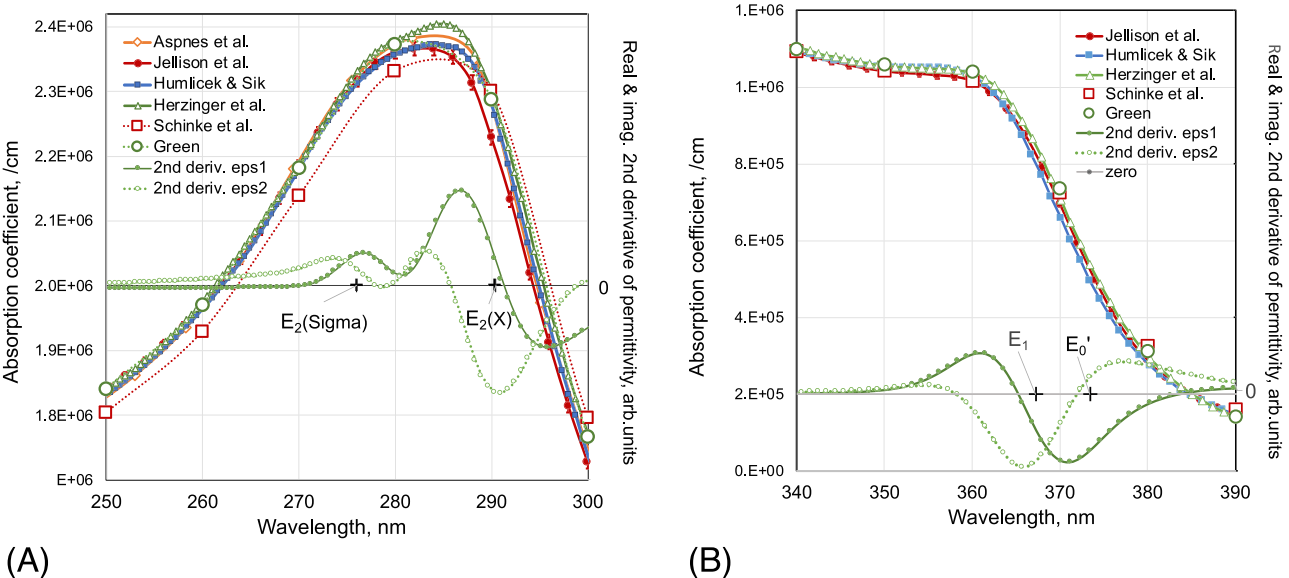


FIGURE 4 Short wavelength absorption coefficient including second derivative of permittivity (with respect to energy) of the Herzinger et al.¹⁹ data showing features due to the critical points indicated, all associated with direct bandgap transitions: (A) 250- to 300-nm range; (B) 340- to 390-nm range

difference formula). The smoothness of these curves demonstrates a high level of data consistency between data points. Cardona et al.¹⁸ (relying upon somewhat noisier data) show how deconvolution of these second derivative curves can be used to deduce the $E_2(X)$ and $E_2(\Sigma)$ critical point energies, their temperature dependencies and the ‘dimensionality’ (D) of the critical point (3D when the three associated effective masses, be they positive or negative or a mixture, have similar magnitudes, 2D or 1D when one has a much higher or lower magnitude than the other 2, respectively, and 0D when the bands are quite flat and parallel in the region involved or the transition is excitonic).

These authors¹⁷ find the transitions largely 2D at the critical points mentioned at room temperature. Subsequent work²² has applied ‘fractional’ differentiation to the permittivities, allowing more precise location of the critical point energy and the assignment of a non-integral dimensionality. Lefebvre et al.²³ state that this non-integral value allows full specification of the permittivities in the vicinity of the critical point, regardless of other parameters. The dimensionality found for the merged E_2 critical points was 1.5 at room temperature, increasing with temperature.²² The Humlíček and Šík⁹ data were also sufficiently dense to allow feature identification via second-order differentiation, with the unsmoothed data giving similar values to those plotted, but with the resulting curves much noisier.

It is immediately obvious from Figure 4A that the Schinke et al.⁶ data, although only 2% different from these earlier datasets, are fundamentally different corresponding to a lower absorption peak shifted to longer wavelengths (to lower energy by 15–34 meV). Additionally, an unusual temperature dependency in this range was reported as previously noted. Multiple earlier measurements^{11,12} show that the absorption peak decreases and shifts to longer wavelengths (lower energy) as temperature increases. This corresponds to negative

temperature coefficients on the low wavelength side of the peak and positive on the long wavelength side.

Schinke et al.⁶ report positive coefficient both sides, corresponding to the peak increasing with increasing temperature. Neither of the above two anomalies was commented upon or apparently investigated⁶ but is suggestive of a systematic issue in data extraction at these wavelengths. Further investigation is clearly warranted before the Schinke et al.⁶ data could be accepted as superior to the consensus established by Figure 4A in this wavelength range. By contrast, the extrapolated Green data are clearly almost a perfect fit to this norm and in good agreement with that of Herzinger et al.,¹⁹ which, given its quality and good agreement with other datasets, is chosen for the tables in both this range and also the following range, where a similar compilation of data is shown in Figure 4B.

The Jellison²¹ data were measured on the heaviest doped samples (Figure 2b). Doping tends to reduce the peak value near 290 nm, as well as at the shoulder associated with the next two lower energy critical points (shown in Figure 4B), consistent with the trend apparent in the Jellison data. Again, the second derivative of the Herzinger et al. data in this second range is very smooth, showing that the features associated with the two critical points, separated in lower temperature data, have merged by this temperature due to broadening (Figure 4B). All data are reasonably consistent over this range, with the extrapolated Green² data too high to be representative on the short wavelength side of Figure 4B, whereas the Schinke et al.⁶ data are too high on the long wavelength side, with the Herzinger et al.¹⁹ data a good compromise.

The next data range (380–500 nm) shown in Figure 5A is at the high energy end of the indirect absorption range and introduces additional issues. The rapidly reducing absorption coefficients (and

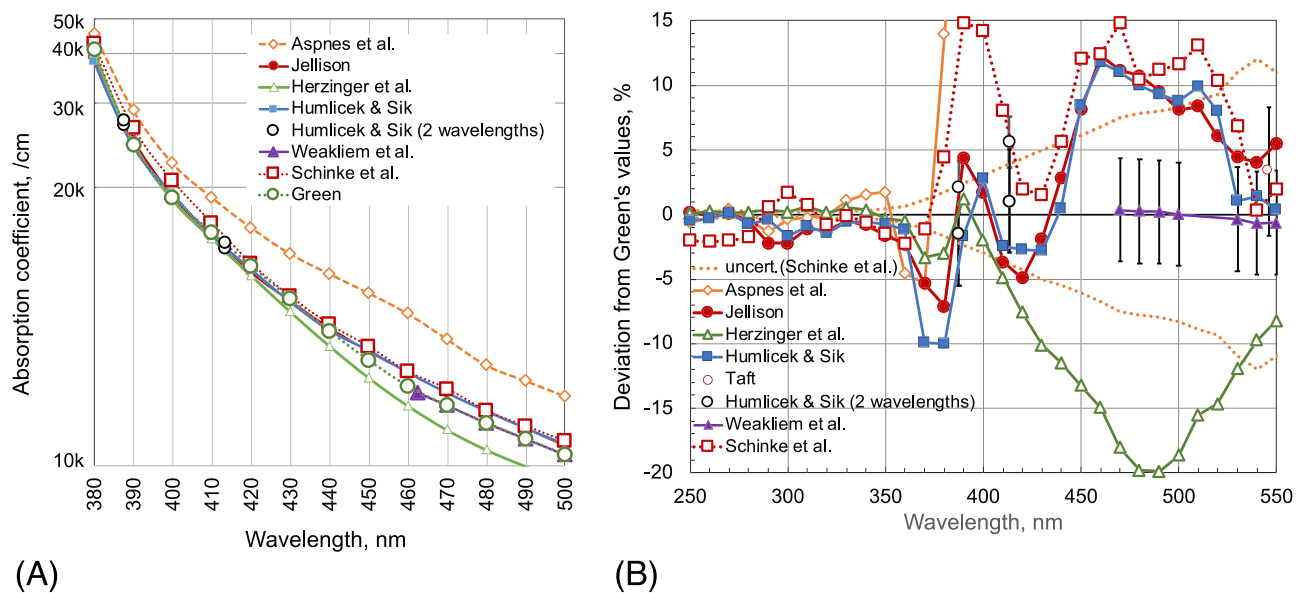


FIGURE 5 (A) Semilogarithmic plot of absorption coefficient versus wavelength over the 380- to 500-nm range at 295 K showing a range of published data mentioned in the text; (B) more detailed plot of the differences between datasets over an extended wavelength range by plotting as the percentage difference from Green's dataset (extrapolated to 295 K). Uncertainty estimates of 5% in the Weakliem and Redfield¹⁰ data, regarded as the most accurate in their wavelength range, are also shown

associated extinction coefficients) with increasing wavelength reduce their impact upon reflection and consequently on the accuracy of ellipsometry and K-K analysis in deducing their values. It also is the region where the maximum percentage disagreement is seen between the Schinke et al.⁶ and extrapolated Green² data of 14%–15% for wavelengths 390 and 400 nm (where the $k = 2$ uncertainty in the Schinke et al. data⁶ is reported as $\leq 3\%$). However, as can be seen from Figure 5A, the Schinke et al.⁶ data appear as outliers with the extrapolated Green data at these wavelengths in reasonably good agreement with the published data of Jellison et al.,²¹ Herzinger et al.,¹⁹ and Humlíček and Šík.⁹ The Aspnes and Studna²⁰ data deviate in the same direction as those of Schinke et al.⁶ but are clear outliers at such wavelengths. Beyond 420 nm, the Herzinger et al.¹⁹ data also become unreliable. Unlike other datasets,^{6,9,21} stabilising long wavelength values of silicon optical properties derived by other techniques were not used to pin down ellipsometric results at these wavelengths. Instead, these properties were allowed to drift as part of the overall fitting routine, resulting in absorption coefficient values that are clearly too low at these wavelengths.

The Jellison²¹ ellipsometric data are firmed at long wavelengths by matching to early transmission measurements by Dash and Newman²⁴ over the 765- to 805-nm range (the latter dataset was not included in the present evaluation because uncertainties were judged too large). The Dash and Newman²⁴ values in this range are about 20% higher than in Green's earlier tabulation, suggesting the Jellison et al.¹¹ data will trend to values that are too high at long wavelengths. The Humlíček and Šík⁹ data are normalised to the transmission data of Weakliem and Redfield,¹⁰ whereas the Schinke et al.⁶ data are normalised to the team's own transmission data, with both these transmission datasets in good agreement with Green's tabulation.²

Not only does the uncertainty associated with ellipsometric measurements increase over this range (both Schinke et al.⁶ and Jellison²¹ estimate $k = 2$ uncertainty increases from 3% at 400 nm to 12%–13% at 540 nm), but also so does that associated with the K-K approach, with Green² switching to reliance on the Weakliem and Redfield¹⁰ transmission data at 470 nm.

A different perspective on the data in Figure 5A is provided by Figure 5B, which shows data over a slightly extended data range relative to Green's extrapolated data.² All datasets are in reasonable agreement from 250 to 360 nm, although there are systematic differences already noted (wavelength offset of the Schinke et al.⁶ data and slightly lower peak for the Jellison²¹ data). Beyond this wavelength, associated with a steep drop in absorption coefficient (Figure 4B), measurements become more challenging as evidenced by the data divergence. The Aspnes and Studna²⁰ data become unusable, while the Schinke et al.⁶ data shoot to a high value while the Humlíček and Šík⁹ data drop to a low value, both relative to Green's data.² (Humlíček and Šík⁹ document much more rapid fluctuations on a wavelength increment scale about 10 times shorter than the 10-nm steps in Figure 5B). Over the 350- to 500-nm range, the weight of data in Figure 5B suggests a low/high/low/high variation with respect to Green's data.

Beyond 430 nm, the Herzinger et al.¹⁹ data lose accuracy quickly and are no longer useful, leaving the Jellison²¹ and the Schinke et al.⁶ ellipsometric datasets, the Humlíček and Šík⁹ data that, beyond 413 nm, switch from ellipsometric to being based on a unique technique using reflection from embedded silicon layers of circa 100-nm thickness. Beyond 528 nm, Humlíček and Šík⁹ regard the most reliable data as provided by transmission measurements by Weakliem and Redfield¹⁰ on silicon specimens thinned to 5.5-micron thickness using

techniques developed for silicon vidicon production, the same data regarded as the most reliable by Green² beyond 470 nm. The Schinke et al.⁶ data also independently converge on values close to Weakliem and Redfield.¹⁰

The absorption coefficient values over the 250- to 500-nm range selected for the revised dataset are the Herzinger et al.¹⁹ values from 250 to 390 nm with a transition to the Humlíček and Šík⁹ data from 400 to 460 nm. Over the 470- to 500-nm range, a smooth, subjective transition is made from the Humlíček and Šík⁹ dataset to values close to those deduced by Weakliem and Redfield,¹⁰ rather than the very abrupt transition between the two made in the Humlíček and Šík⁹ dataset. The 450- to 500-nm range is the region of maximum uncertainty in the combined dataset for wavelengths that correspond to energies above the bandgap, due to the divergences between available datasets in this region, as apparent in Figure 5B.

4.3 | Mid-wavelength region (500–1150 nm)

Over the 500- to 1050-nm range, absorption is dominated by absorption with momentum conserving TO phonon emission with no other strong absorption features over this range. Geist²⁵ has deduced an analytical expression that provides a good baseline for evaluating different datasets over this range at room temperature. One advantage of a smooth and reasonably accurate analytical baseline over a region where there are no abrupt absorption features is that it can illuminate

random errors in the different datasets, evident as oscillations with wavelength (see Figure 6).

Figure 6 shows some key datasets considered in this work relative to the Geist analytical baseline.²⁵ At the short wavelength end are the three datasets already discussed but looking a little different referenced to a smooth baseline. The Schinke et al.⁶ data oscillate strongly at these wavelengths as ellipsometry struggles with maintaining accuracy. A large discontinuity is apparent in the Humlíček and Šík⁹ data due to a switch in the data source, as previously noted. The Weakliem and Redfield¹⁰ data are far less noisy but dive precipitously relative to the Geist expression²⁵ at the short wavelengths. This does not imply the Weakliem and Redfield¹⁰ data are any less accurate at these wavelengths than at longer wavelengths, where their accuracy has been endorsed by Geist. It could just mean that the Geist expression is inaccurate at these wavelengths since fitted to the Jellison²¹ dataset, which is also struggling at these wavelengths, and additionally likely to be high since normalised to Dash and Newman²⁴ data.

Despite the uncertainty in the Schinke et al.⁶ data being large at 650 nm, reaching its maximum value of 13%, these data are in good agreement with other independent data with lower uncertainty at these wavelengths, namely, the transmission data of Geist,²⁵ Weakliem and Redfield¹⁰ and Wang et al.²⁶ This may be fortuitous given the large fluctuations apparent in the Schinke et al.⁶ data below 650 nm. Beyond 650 nm, the fluctuations relative to the Geist analytical expression are completely eliminated. This is due to the approach

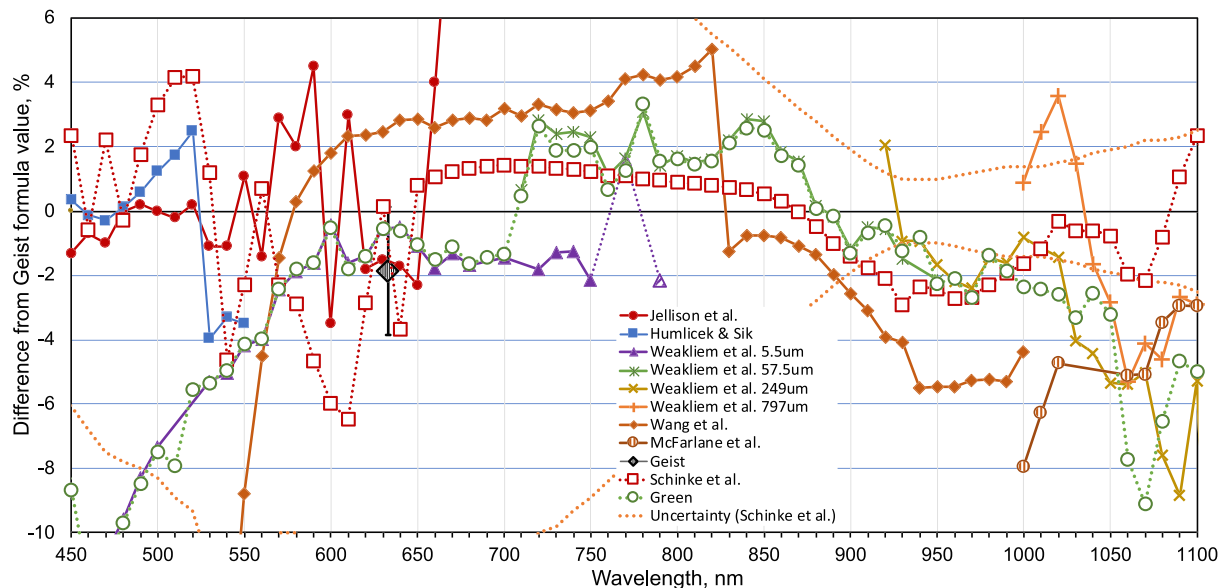


FIGURE 6 Plot of absorption coefficient values relative to the analytical expression deduced by Geist,²⁵ based largely on the Jellison²¹ ellipsometric dataset at short wavelengths and the data of Weakliem and Redfield¹⁰ at longer wavelengths. The latter are deduced from transmission measurements on four wafers with thickness ranging from 5.5 to 797 μm . Similar transmission data are also shown from Wang et al.²⁶ for three wafers ranging in thickness from 10 to 110 μm and from McFarlane et al.¹⁶ for wafers ranging in thickness from 249 μm to 1.77 cm. The scatter for each dataset is indicative of random errors, becoming large for the ellipsometric measurements shown at these wavelengths, but relatively small for the transmission measurements. Discontinuities become apparent when plotted this way, notably in both the Humlíček and Šík⁹ data as noted in the text and also in the Wang et al.²⁶ data (change in wafer thickness in the latter case)

used in deducing the Schinke et al.⁶ data, essentially relying on mathematical interpolation between 650 and 930 nm. This smooth interpolation is seen to provide an excellent fit to independently measured data over this range. The Schinke et al.⁶ data have very low uncertainty from 900 to 1050 nm allowing use as a baseline to normalise earlier data, with a plot over the 650- to 1150-nm range so normalised shown in Figure 7.

Below 910 nm, the three datasets shown all lie within the Schinke et al.⁶ uncertainty range. Because the Schinke et al.⁶ data are described by a mathematical formula, any apparent wavelength fluctuations arise from the other datasets and give an indication of random (Type 2) errors, which seem to be below 1% (rms) for all three datasets over at least a significant part of their range. Beyond 920 nm, the Schinke et al.⁶ data also contribute to these fluctuations and enhance the fluctuation apparent in the plotted Wang et al.²⁶ data at 930 nm.

Wang et al.²⁶ also include uncertainty estimates ($k = 2$) ranging from 5% to 9% at long wavelengths. A similar uncertainty range is estimated for the Weakliem and Redfield¹⁰ data. These demonstrate an abrupt increase in the level of fluctuation at long wavelengths for all four samples. This was traced to the transition from wavelengths where light was relatively strongly absorbed so a single pass of light across the sample (solid curves) determined sample transmission to the case where multiple passes across the sample contributed (dotted curves). Sample non-idealities such as non-parallel surfaces and thickness variation may have increased noise levels in such cases due to non-identical optical pathlengths for neighbouring data points.

Another feature common to both Wang et al.²⁶ and Weakliem and Redfield¹⁰ data is an apparently random jump in baseline values for samples of different thicknesses, with typical jumps of 5%–6%, a major contributor to the uncertainty estimates (at longer wavelengths, use of wafers with different doping levels may contribute to these jumps, as indicated by Figure 2B). However, the above data support the view that, in the 650- to 1000-nm range, the actual absorption coefficient for lightly doped samples is within $\pm 4\%$ of the Schinke

et al. values with above 95% certainty, with the final uncertainty estimates ($k = 2$) capped at this value over this range. The Schinke et al.⁶ absorption coefficient values will be used for the revised dataset over the 650- to 1150-nm range, apart from a slight increase in the value at 930 nm by 0.4% to reduce the random fluctuation apparent in Figures 6 and 7.

4.4 | Long-wavelength region (1150–1450 nm)

Datasets taken into account over this long wavelength range are shown on a logarithmic scale in Figure 8A. The first distinctive dip apparent circa 1180 nm is due to the onset of absorption of a photon of this wavelength and a momentum conserving TO phonon. Another dip is apparent at circa 1260 nm, due to onset of absorption of a photon and two phonons. One is the same momentum conserving TO phonon, and the second is the zone centre, Raman active optical phonon. A third dip is apparent at circa 1350 nm, a replica of the previous dip, but due to onset of absorption of a photon and three phonons (the momentum conserving TO phonon and two zone centre, Raman active optical phonons). Note that the absorption coefficient decreases by an almost constant factor in the 100- to 200-range between each of these dips. Second-order perturbation would predict this behaviour together with a sequence of further dips extending to even longer wavelengths.¹⁸

Due to the approximately constant factor between dips, an exponentially decreasing baseline can be fitted to the absorption coefficient as indicated in Figure 8A with the departure of experimental data from this baseline plotted as in Figure 8B (the baseline was chosen to highlight the similarity between phonon replicas). This highlights that, beyond 1350 nm, the experimental data are not behaving as expected. Although the Green 2008 revised data and those of Schinke et al.⁶ are in reasonably good agreement at these wavelengths, examination of the raw experimental data shows both

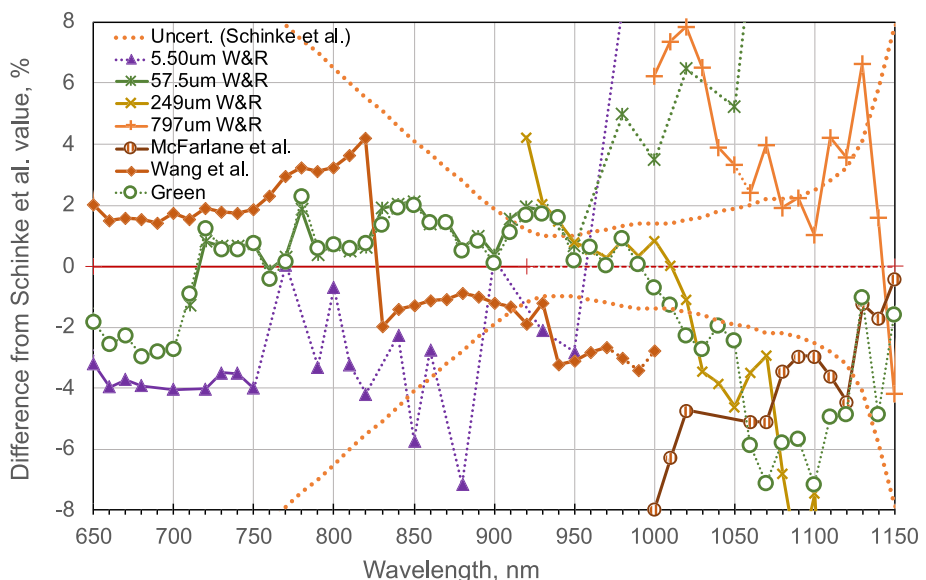


FIGURE 7 Plot of absorption coefficient datasets of Figure 6 normalised to the experimental dataset of Schinke et al.⁶ suggesting this dataset provides a better fit to the other datasets indicated over the 650- to 1150-nm range than does the analytical expression suggested by Geist.²⁵ Uncertainty estimates provided by Schinke et al.⁶ also seem realistic beyond 900 nm but are likely too conservative below this wavelength when the other datasets are taken into account

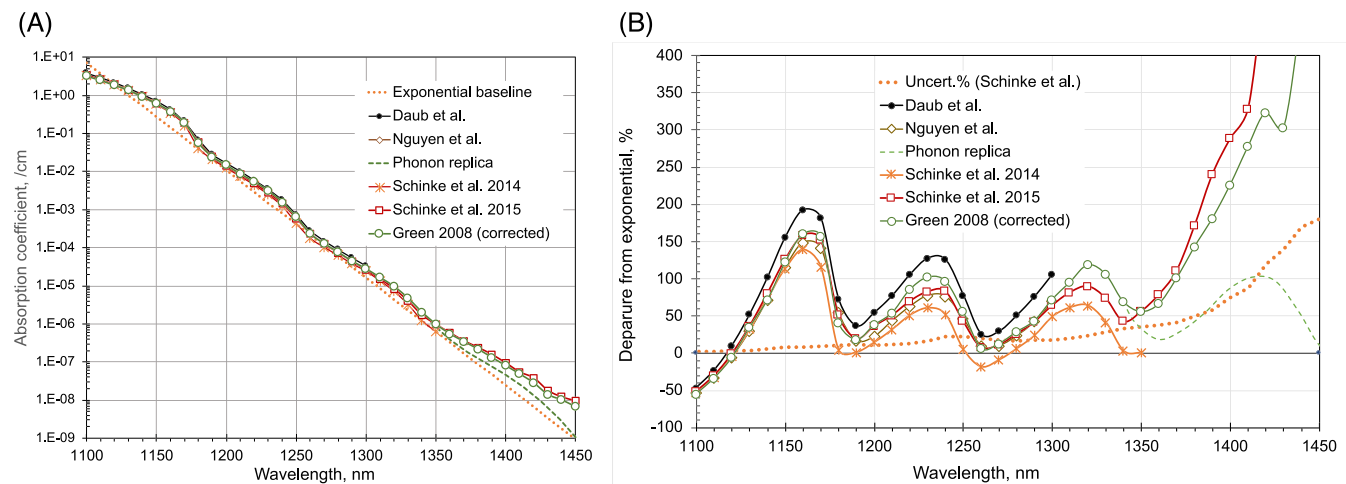


FIGURE 8 (A) Sub-bandgap absorption coefficient of silicon as deduced by different authors. Also shown is an exponentially decreasing baseline and, beyond 1350 nm, an estimation of absorption coefficient value based on phonon replica theory; (B) departure of absorption coefficient values from the exponential baseline highlighting the phonon replicas and differences in values deduced by different researchers

datasets are becoming very noisy in this range with rapidly increasing uncertainty estimates. By plotting Figure 8B versus energy and shifting the ‘clean’ two phonon replica at 1200–1250 nm to lower energy by two Raman phonon energies (130 meV), an approximation to the theoretically expected behaviour is deduced and is plotted as the green dashed line in Figure 8A,B.

The departure from theoretical expectations suggests measurements beyond 1350 nm are increasingly dominated by noise or defect-assisted multiple step transitions, such as apparent at lower energy in the work of Anagnostopoulos and Sadasiv²⁷ and, for samples damaged by ion implantation, in the work of Keevers and Green.²⁸ Moreover, measurements give much higher values than theoretically expected suggesting both sets of experimental data are likely to be high in this wavelength range.

Over the 1190- to 1450-nm range, the datasets of Green² and Schinke et al.⁶ have been independently derived by different techniques (spectral response of high-performance solar cells and photoluminescence response of textured wafers, respectively). They would be likely to have similar associated uncertainty and are compatible within this uncertainty range. The approach taken over the 1190- to 1350-nm range was to take the average of the two datasets, while reducing the associated uncertainty from the value assigned by Schinke et al.⁶ The procedure used in estimating tabulated values beyond 1350 nm was to take into account the likelihood that the experimental data are overestimates, for the reasons noted. Noting the accuracy of the phonon replica approach over the 1280- to 1350-nm wavelength range, the procedure adopted was to give this approach equal weight with the experimental data over the 1360- to 1450-nm range in deducing the tabulated value. The higher of the two datasets was then taken as the upper bound on experimental absorption coefficient values with 95% confidence, with uncertainty ($k = 2$) estimated as the percentage difference between this and the tabulated value.

4.5 | Summary of selected 295-K absorption data

Based on the above review, the final 295-K absorption coefficient dataset over the 250- to 390-nm range consists of the Herzinger et al.¹⁹ data; from 400 to 460 nm, those of Humlíček and Šík⁹; from 470 to 570 nm, the latter progressively weighted by those of Weakliem and Redfield¹⁰; from 580 to 640 nm, a weighting of Weakliem and Redfield¹⁰ data and those of Wang et al.²⁶; from 650 to 1150 nm, the data of Schinke et al.⁶ (with a 0.4% increase at 930 nm); from 1160 to 1350 nm, the average of the Schinke et al.⁶ data and the revised data of Green²; and from 1360 to 1450 nm, the average of the latter and that deduced for the phonon replica.

Uncertainty estimates relied upon those of Schinke et al.⁶ as a benchmark, as shown in Figure 9, increasing these to those of Jellison²¹ over the 250- to 400-nm range due to a fundamental inconsistency in datasets over this range (Figures 4 and 5). They were capped at 10% from 530 to 570 nm, decreasing to a cap of 4% from 650 to 850 nm due to a high level of consistency between different datasets (Figures 6 and 7). From 1150 to 1350 nm, estimates were reduced to accommodate complementary data with similar associated uncertainty (Figure 8), with values in the 1360- to 1450-nm range determined from the difference between the tabulated value and the most extreme of the three values used in its determination, as previously described.

5 | ABSORPTION COEFFICIENT TEMPERATURE DEPENDENCY

Below 1050 nm where absorption is either direct or involves phonon emission, optical properties would not be expected to be as temperature dependent as beyond 1050 nm where phonon absorption is involved. This differentiation is apparent in the data of Figure 1.

The main source of temperature coefficient data in the first range is Jellison and Modine,¹¹ considered reliable given the reasonable agreement with other datasets, and also of Weakliem and Redfield.¹⁰ The data of Schinke et al.⁶ are based on ellipsometry measurements and, although in reasonable agreement with these other data sources, was not taken into account due to the unresolved issues in this wavelength range previously noted.

Some systematic trends in the temperature dependence of absorption coefficient have been previously noted. Jellison and

Modine¹¹ observed an exponential dependence on temperature below the direct bandgap while Svantesson and Nilsson²⁹ observed a power law dependence at longer wavelengths where absorption of both a photon and a phonon was involved. The temperature variation of a parameter p can be expressed in terms of a normalised temperature coefficient, c_p , defined at temperature T_0 as²:

$$c_p = \frac{1}{p} \frac{dp}{dT} \Big|_{T_0} = \frac{d(\ln p)}{dT} \Big|_{T_0}. \quad (1)$$

For the normally assumed linear variation with temperature:

$$p(T_0 + \Delta T) = p(T_0)(1 + c_p \Delta T), \quad (2)$$

while for an exponential dependence:

$$p(T_0 + \Delta T) = p(T_0) \exp(c_p \Delta T), \quad (3)$$

and for a power law dependence:

$$p(T_0 + \Delta T) = p(T_0)(T/T_0)^{c_p T_0}. \quad (4)$$

The latter two equations expand to the same form as Equation 2 for small ΔT . However, higher order terms become important for larger ΔT . These latter equations have the advantage that they can never change the sign of p , no matter how large the extrapolation, as physically expected.

The extensive dataset of Nguyen et al.⁴ allow the transition from exponential to power law dependence to be investigated. Figure 10 shows absorption coefficient versus temperature for a subset of these data for temperatures in the range of 170–363 K. Shown as the variable is the photon wavelength, ranging from 990 to 1300 nm in 5-nm steps. Also shown are least square fits to the data generally in 20-nm

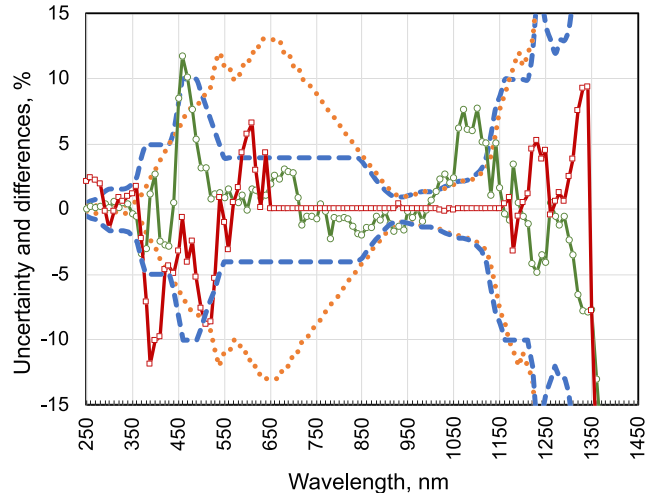


FIGURE 9 Estimated percentage uncertainty (coverage factor $k = 2$) in tabulated absorption coefficient values for the present dataset (blue dashed line) compared to that of Schinke et al.⁶ (orange dotted line). Also shown as the solid lines is the percentage difference between the new dataset and the earlier published datasets of Green² (revised; green line, round marker) and of Schinke et al.⁶ (red line, square marker)

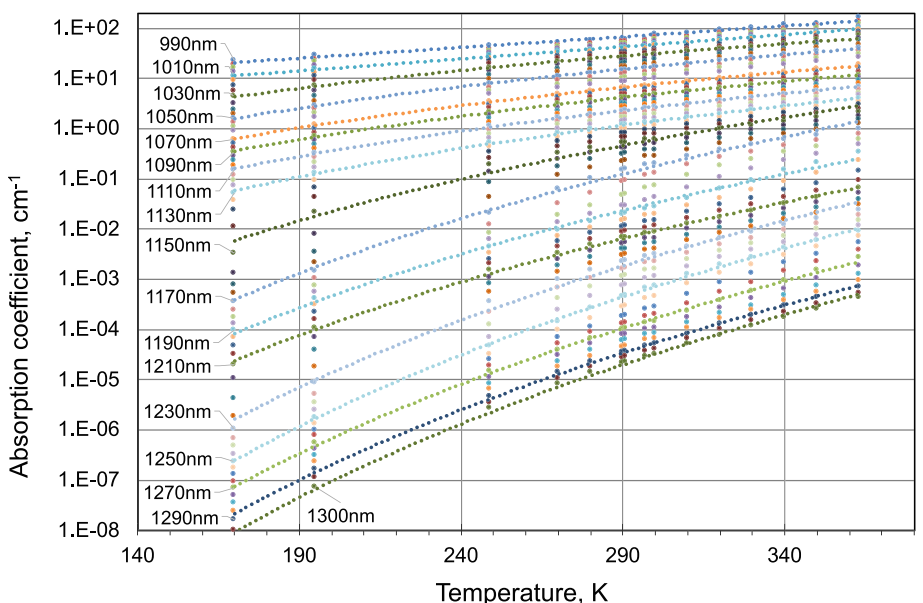


FIGURE 10 Absorption coefficient values of Nguyen et al.⁴ at different wavelengths plotted as a function of absolute temperature from 170 to 363 K and fitted by an exponential fit from 990 to 1030-nm wavelength and a power law fit from 1030 to 1300 nm. The fit chosen in all cases was that giving the highest coefficient of determination

steps. The coefficient of determination, R^2 , for each of these fits is very close to unity. For the 18 fits shown, the lowest value is 0.97 for the 990-nm fit, possibly because the corresponding values may be the least reproducible, since at the edge of the measurement range. Eight of the 18 fits have R^2 values in the 0.990–0.998 range, with another eight with values 0.999–1.000.

For wavelengths in the 990- to 1030-nm range, an exponential fit gave the highest coefficient of determination while, for the 1030- to 1300-nm range, a power law fit gave the highest value, with the different ranges corresponding roughly to photon absorption with phonon emission for the first range and with phonon absorption for the second.

The plot also suggests that extrapolation over a large temperature range is feasible, if fits from plots like these are used to deduce temperature coefficients. The values so deduced may differ from those derived from direct differentiation at any specific temperature, particularly near absorption thresholds. Temperature coefficient values from fits such as in Figure 10 are tabulated to allow long-range extrapolation, with the corresponding disadvantage being that temperature variations of thresholds may not be accurately modelled. An alternative may be to calculate the energy derivative of the absorption coefficient at the reference temperature and use Figure 2A to estimate the local value of the temperature coefficient at this temperature to better model such shifts, although this approach would not be conducive to long-range extrapolation.

A comparison of long- and short-range extrapolation coefficients deduced from the Nguyen et al.⁴ data at 295-K reference temperature is shown in Figure 11. The long-range values were extracted from the exponential and power law fits to the data of Figure 10 using Equations 3 and 4, respectively. The short-range values were obtained by

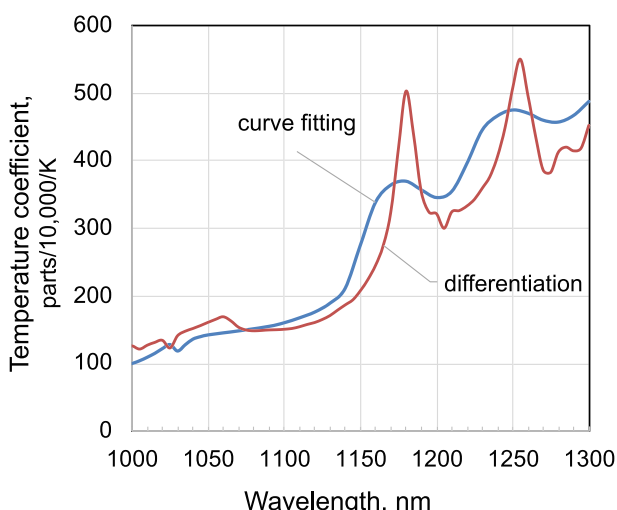


FIGURE 11 Temperature coefficient of silicon's absorption coefficient at 295 K as deduced from the data of Nguyen et al.⁴ both by differentiating the polynomial fit to absorption coefficient provided by these authors and from the curve fits shown in Figure 10 over the 170- to 363-K range

direct differentiation of the fifth-order polynomial used by Nguyen et al.⁴ to fit the temperature dependence over the 170- to 363-K range at each wavelength. The long-range values appear to be broadened versions of the short-range values with peaks slightly blue-shifted, likely due to the inclusion of a wider range of temperatures below 295 K in the long-range fit than above this temperature.

6 | 25°C AND 300-K ABSORPTION COEFFICIENT DATASETS

Using the above improved understanding of temperature dependencies, the refined 295-K absorption coefficient dataset was extrapolated to both 25°C and 300 K. Values at all three temperatures are tabulated in Table 1, with the values at 25°C most relevant to photovoltaic device simulation and performance specification. Also tabulated are the ‘long-range’ values of the normalised temperature coefficient at 25°C. From the exponential temperature dependence in the indirect absorption region with phonon emission, it follows from Equation 3 that the temperature coefficient should not be strongly temperature dependent in this range, as also likely a reasonable assumption in the direct absorption region. Equation 3 would be a reasonable way of extrapolating data for both regions.

In the long wavelength region, where absorption requires simultaneous absorption of a phonon, extrapolation presents more challenges as already noted. Using Equation 4 and the tabulated temperature coefficients, long-range extrapolations are feasible as rough estimates of the expected values, to an accuracy suggested by Figure 10, and some actual results shown elsewhere.² Over the 990- to 1300-nm wavelength range, the data and approach of Nguyen et al.⁴ will provide potentially more accurate data, despite the narrower bandgap expected from the high injection levels. Although not used in data compilation at 295 K due to the inability to correct for this narrowing, values at 295 K differed from those of both Schinke et al.⁶ and ‘Green 2008 revised’ by less than 15% over this restricted range (Figure 8B). Similar accuracy maybe expected at temperatures above room temperature although, below room temperature, increased bandgap narrowing for a given injection level would be expected to increase departure from values for more moderate injection levels.¹³

7 | REFRACTIVE INDEX

Since the earlier tabulations,^{1,2} the real part of silicon's refractive index at long wavelengths (1100–5600 nm) and its temperature dependence over the 20- to 300-K range have been determined with reduced uncertainty of typically better than 30 ppm (parts per million).⁸ Values of both the index and its temperature coefficient at 25°C are tabulated over the 1100- to 1450-nm range in Table 1 from this source. Values remain unchanged to four significant digits at both 295 and 300 K, with use of the tabulated temperature coefficients giving the reported values to five significant digits.

TABLE 1 Optical properties of lightly doped silicon

| Wavelength, nm | Alpha, cm ⁻¹ (25°C) | Alpha, cm ⁻¹ (295 K) | Alpha, cm ⁻¹ (300 K) | Uncertainty alpha, % (k = 2) | Normalised T coefficient, 10 ⁻⁴ /K (alpha 25°C) | Real index ^a , n (25°C) | Uncertainty, n % (k = 2) | Normalised T coefficient, 10 ⁻⁴ /K (n 25°C) |
|----------------|--------------------------------|---------------------------------|---------------------------------|------------------------------|--|------------------------------------|--------------------------|--|
| 250 | 1.841E6 | 1.842E6 | 1.841E6 | 0.5 | -0.9 | 1.664 | 1.5 | 2.9 |
| 260 | 1.975E6 | 1.976E6 | 1.975E6 | 0.7 | -1.5 | 1.754 | 1.7 | 2 |
| 270 | 2.185E6 | 2.187E6 | 2.184E6 | 0.8 | -3.1 | 2.087 | 1.7 | 0 |
| 280 | 2.376E6 | 2.378E6 | 2.374E6 | 1.1 | -3.3 | 2.961 | 1.8 | -4.8 |
| 290 | 2.299E6 | 2.298E6 | 2.299E6 | 1.4 | 0.8 | 4.386 | 1.8 | -9 |
| 300 | 1.771E6 | 1.770E6 | 1.772E6 | 1.6 | 2.5 | 5.099 | 1.8 | -3.8 |
| 310 | 1.468E6 | 1.467E6 | 1.469E6 | 1.6 | 3.2 | 5.118 | 1.7 | -1.6 |
| 320 | 1.301E6 | 1.300E6 | 1.301E6 | 1.6 | 1.5 | 5.139 | 1.7 | -1.3 |
| 330 | 1.185E6 | 1.185E6 | 1.185E6 | 1.6 | 0.7 | 5.209 | 1.6 | -1.2 |
| 340 | 1.104E6 | 1.104E6 | 1.104E6 | 1.7 | 0.3 | 5.323 | 1.5 | -1 |
| 350 | 1.056E6 | 1.056E6 | 1.056E6 | 2 | 0 | 5.524 | 1.4 | -1.8 |
| 360 | 1.035E6 | 1.035E6 | 1.034E6 | 2.5 | -1.4 | 6.062 | 1.3 | -4.1 |
| 370 | 7.117E6 | 7.107E5 | 7.122E5 | 4 | 4.2 | 6.960 | 1.3 | -4.4 |
| 380 | 3.031E5 | 3.022E5 | 3.036E5 | 5 | 9.2 | 6.650 | 1.2 | -2.3 |
| 390 | 1.440E5 | 1.428E5 | 1.447E5 | 5 | 26 | 6.058 | 1.2 | 1 |
| 400 | 9.496E4 | 9.397E4 | 9.555E4 | 5 | 33 | 5.630 | 1.2 | 2.1 |
| 410 | 6.738E4 | 6.672E4 | 6.777E4 | 5 | 31 | 5.345 | 1.1 | 2.1 |
| 420 | 5.097E4 | 5.050E4 | 5.124E4 | 5 | 29 | 5.133 | 1.1 | 1.9 |
| 430 | 3.885E4 | 3.849E4 | 3.906E4 | 5 | 29 | 4.962 | 1.0 | 1.8 |
| 440 | 3.069E4 | 3.042E4 | 3.08E40 | 6 | 28 | 4.818 | 0.9 | 1.7 |
| 450 | 2.601E4 | 2.578E4 | 2.615E4 | 8 | 28 | 4.697 | 0.8 | 1.6 |
| 460 | 2.167E4 | 2.147E4 | 2.179E4 | 10 | 29 | 4.592 | 0.6 | 1.6 |
| 470 | 1.819E4 | 1.802E4 | 1.829E4 | 10 | 29 | 4.502 | 0.5 | 1.5 |
| 480 | 1.542E4 | 1.527E4 | 1.550E4 | 10 | 30 | 4.423 | 0.4 | 1.4 |
| 490 | 1.321E4 | 1.308E4 | 1.328E4 | 10 | 30 | 4.355 | 0.3 | 1.4 |
| 500 | 11 380 | 11 270 | 11 450 | 9 | 31 | 4.295 | 0.2 | 1.3 |
| 510 | 9948 | 9850 | 10 010 | 8 | 31 | 4.241 | 0.2 | 1.3 |
| 520 | 8819 | 8730 | 8872 | 7 | 32 | 4.194 | 0.2 | 1.2 |
| 530 | 7893 | 7810 | 7941 | 6 | 33 | 4.151 | 0.2 | 1.2 |
| 540 | 7094 | 7020 | 7138 | 5 | 33 | 4.112 | 0.2 | 1.2 |
| 550 | 6407 | 6340 | 6446 | 4 | 33 | 4.077 | 0.2 | 1.1 |
| 560 | 5833 | 5770 | 5870 | 4 | 34 | 4.045 | 0.2 | 1.1 |
| 570 | 5317 | 5260 | 5351 | 4 | 34 | 4.015 | 0.2 | 1.1 |
| 580 | 4873 | 4820 | 4903 | 4 | 34 | 3.988 | 0.2 | 1.1 |
| 590 | 4509 | 4460 | 4537 | 4 | 34 | 3.963 | 0.2 | 1 |
| 600 | 4145 | 4100 | 4171 | 4 | 34 | 3.940 | 0.2 | 1 |
| 610 | 3833 | 3790 | 3857 | 4 | 35 | 3.918 | 0.2 | 1 |
| 620 | 3549 | 3510 | 3572 | 4 | 35 | 3.898 | 0.2 | 1 |
| 630 | 3286 | 3250 | 3308 | 4 | 35 | 3.879 | 0.2 | 1 |
| 640 | 3044 | 3010 | 3064 | 4 | 35 | 3.861 | 0.2 | 1 |
| 650 | 2824 | 2793 | 2843 | 4 | 35 | 3.844 | 0.2 | 0.9 |
| 660 | 2620 | 2591 | 2637 | 4 | 35 | 3.829 | 0.2 | 0.9 |
| 670 | 2430 | 2402 | 2446 | 4 | 36 | 3.814 | 0.2 | 0.9 |
| 680 | 2252 | 2226 | 2267 | 4 | 36 | 3.800 | 0.2 | 0.9 |
| 690 | 2085 | 2061 | 2099 | 4 | 36 | 3.787 | 0.2 | 0.9 |

(Continues)

TABLE 1 (Continued)

| Wavelength, nm | Alpha, cm ⁻¹ (25°C) | Alpha, cm ⁻¹ (295 K) | Alpha, cm ⁻¹ (300 K) | Uncertainty alpha, % (k = 2) | Normalised T coefficient, 10 ⁻⁴ /K (alpha 25°C) | Real index ^a , n (25°C) | Uncertainty, n % (k = 2) | Normalised T coefficient, 10 ⁻⁴ /K (n 25°C) |
|-------------------|--------------------------------------|---------------------------------------|---------------------------------------|------------------------------------|--|--|-----------------------------|--|
| 700 | 1930 | 1907 | 1943 | 4 | 37 | 3.774 | 0.1 | 0.9 |
| 710 | 1784 | 1763 | 1796 | 4 | 37 | 3.763 | 0.1 | 0.9 |
| 720 | 1648 | 1629 | 1660 | 4 | 37 | 3.751 | 0.1 | 0.9 |
| 730 | 1521 | 1503 | 1531 | 4 | 37 | 3.741 | 0.1 | 0.8 |
| 740 | 1402 | 1386 | 1412 | 4 | 37 | 3.731 | 0.1 | 0.8 |
| 750 | 1291 | 1276 | 1300 | 4 | 37 | 3.721 | 0.1 | 0.8 |
| 760 | 1187 | 1173 | 1195 | 4 | 37 | 3.712 | 0.1 | 0.8 |
| 770 | 1091 | 1078 | 1098 | 4 | 37 | 3.703 | 0.1 | 0.8 |
| 780 | 1000 | 988.2 | 1007 | 4 | 37 | 3.695 | 0.1 | 0.8 |
| 790 | 915.9 | 904.9 | 922.4 | 4 | 38 | 3.687 | 0.1 | 0.8 |
| 800 | 837.7 | 827.1 | 844.0 | 4 | 40 | 3.679 | 0.1 | 0.8 |
| 810 | 764.5 | 754.6 | 770.4 | 4 | 41 | 3.672 | 0.1 | 0.8 |
| 820 | 696.4 | 687.1 | 701.8 | 4 | 42 | 3.665 | 0.1 | 0.8 |
| 830 | 633.1 | 624.3 | 638.3 | 4 | 44 | 3.658 | 0.1 | 0.7 |
| 840 | 574.1 | 565.9 | 578.9 | 4 | 45 | 3.652 | 0.1 | 0.7 |
| 850 | 519.2 | 511.6 | 523.6 | 3.7 | 46 | 3.645 | 0.1 | 0.7 |
| 860 | 468.2 | 461.2 | 472.3 | 3.2 | 47 | 3.639 | 0.1 | 0.7 |
| 870 | 421.0 | 414.5 | 424.9 | 2.8 | 49 | 3.634 | 0.1 | 0.7 |
| 880 | 377.4 | 371.3 | 381 | 2.3 | 51 | 3.628 | 0.1 | 0.7 |
| 890 | 336.8 | 331.3 | 340.1 | 1.9 | 52 | 3.623 | 0.1 | 0.7 |
| 900 | 299.6 | 294.5 | 302.6 | 1.5 | 54 | 3.618 | 0.1 | 0.7 |
| 910 | 265.2 | 260.5 | 268 | 1.2 | 56 | 3.613 | 0.1 | 0.7 |
| 920 | 233.5 | 229.3 | 236 | 1 | 57 | 3.608 | 0.1 | 0.7 |
| 930 | 203.2 | 199.4 | 205.4 | 1 | 59 | 3.604 | 0.1 | 0.7 |
| 940 | 178.1 | 174.6 | 180.1 | 1 | 62 | 3.599 | 0.1 | 0.7 |
| 950 | 153.9 | 150.7 | 155.7 | 1.1 | 65 | 3.595 | 0.1 | 0.7 |
| 960 | 131.5 | 128.6 | 133.2 | 1.2 | 69 | 3.591 | 0.1 | 0.7 |
| 970 | 111.5 | 108.9 | 113 | 1.3 | 73 | 3.587 | 0.1 | 0.7 |
| 980 | 93.77 | 91.47 | 95.17 | 1.4 | 78 | 3.583 | 0.1 | 0.7 |
| 990 | 77.73 | 75.70 | 78.94 | 1.4 | 84 | 3.579 | 0.1 | 0.7 |
| 1000 | 63.39 | 61.60 | 64.46 | 1.4 | 91 | 3.575 | 0.08 | 0.7 |
| 1010 | 50.84 | 49.29 | 51.77 | 1.5 | 98 | 3.571 | 0.07 | 0.7 |
| 1020 | 40.02 | 38.73 | 40.80 | 1.6 | 106 | 3.568 | 0.06 | 0.7 |
| 1030 | 30.36 | 29.34 | 31.00 | 1.8 | 113 | 3.565 | 0.05 | 0.7 |
| 1040 | 22.55 | 21.7 | 23.05 | 1.9 | 121 | 3.562 | 0.04 | 0.6 |
| 1050 | 16.29 | 15.61 | 16.70 | 2 | 136 | 3.559 | 0.04 | 0.6 |
| 1060 | 11.52 | 10.96 | 11.83 | 2.2 | 146 | 3.556 | 0.03 | 0.6 |
| 1070 | 8.374 | 7.965 | 8.618 | 2.2 | 156 | 3.553 | 0.03 | 0.6 |
| 1080 | 6.387 | 6.070 | 6.580 | 2.3 | 161 | 3.550 | 0.03 | 0.6 |
| 1090 | 4.827 | 4.585 | 4.977 | 2.5 | 166 | 3.547 | 0.03 | 0.6 |
| 1100 | 3.648 | 3.452 | 3.768 | 2.8 | 176 | 3.5445 | 0.006 | 0.60 |
| 1110 | 2.743 | 2.594 | 2.836 | 3.2 | 181 | 3.5421 | 0.006 | 0.60 |
| 1120 | 2.037 | 1.915 | 2.108 | 4.1 | 186 | 3.5398 | 0.006 | 0.60 |
| 1130 | 1.466 | 1.377 | 1.519 | 5.8 | 191 | 3.5375 | 0.006 | 0.60 |
| 1140 | 1.013 | 0.950 | 1.051 | 7.8 | 201 | 3.5352 | 0.006 | 0.60 |

TABLE 1 (Continued)

| Wavelength, nm | Alpha, cm ⁻¹ (25°C) | Alpha, cm ⁻¹ (295 K) | Alpha, cm ⁻¹ (300 K) | Uncertainty alpha, % (k = 2) | Normalised T coefficient, 10 ⁻⁴ /K (alpha 25°C) | Real index ^a , n (25°C) | Uncertainty, n % (k = 2) | Normalised T coefficient, 10 ⁻⁴ /K (n 25°C) |
|----------------|--------------------------------|---------------------------------|---------------------------------|------------------------------|--|------------------------------------|--------------------------|--|
| 1150 | 0.663 | 0.622 | 0.689 | 8.8 | 211 | 3.5331 | 0.006 | 0.59 |
| 1160 | 0.401 | 0.373 | 0.418 | 10 | 231 | 3.5310 | 0.006 | 0.59 |
| 1170 | 0.208 | 0.191 | 0.218 | 10 | 262 | 3.5289 | 0.006 | 0.58 |
| 1180 | 0.0634 | 0.0572 | 0.0673 | 10 | 322 | 3.5269 | 0.006 | 0.58 |
| 1190 | 0.0272 | 0.0243 | 0.0289 | 10 | 347 | 3.5250 | 0.006 | 0.58 |
| 1200 | 1.64E-2 | 1.46E-2 | 1.75E-2 | 10 | 357 | 3.5231 | 0.006 | 0.57 |
| 1210 | 9.59E-3 | 8.49E-3 | 1.03E-2 | 10 | 382 | 3.5213 | 0.006 | 0.57 |
| 1220 | 5.85E-3 | 5.16E-3 | 6.290E-3 | 12 | 392 | 3.5195 | 0.006 | 0.57 |
| 1230 | 3.32E-3 | 2.92E-3 | 3.580E-3 | 16 | 408 | 3.5178 | 0.006 | 0.57 |
| 1240 | 1.72E-3 | 1.51E-3 | 1.850E-3 | 16 | 413 | 3.5161 | 0.006 | 0.56 |
| 1250 | 7.08E-4 | 6.18E-4 | 7.67E-4 | 14 | 433 | 3.5144 | 0.006 | 0.56 |
| 1260 | 2.67E-4 | 2.32E-4 | 2.89E-0 | 13 | 443 | 3.5128 | 0.006 | 0.56 |
| 1270 | 1.46E-4 | 1.26E-4 | 1.59E-4 | 12 | 458 | 3.5112 | 0.006 | 0.56 |
| 1280 | 8.69E-5 | 7.48E-5 | 9.48E-5 | 13 | 473 | 3.5097 | 0.006 | 0.56 |
| 1290 | 5.15E-5 | 4.39E-5 | 5.65E-5 | 13 | 503 | 3.5082 | 0.006 | 0.56 |
| 1300 | 3.19E-5 | 2.70E-5 | 3.51E-5 | 14 | 528 | 3.5067 | 0.005 | 0.55 |
| 1310 | 1.88E-5 | 1.58E-5 | 2.08E-5 | 17 | 553 | 3.5053 | 0.005 | 0.55 |
| 1320 | 1.07E-5 | 8.9E-6 | 1.20E-5 | 20 | 584 | 3.5039 | 0.005 | 0.55 |
| 1330 | 5.3E-6 | 4.3E-6 | 5.9E-06 | 23 | 614 | 3.5026 | 0.005 | 0.55 |
| 1340 | 2.3E-6 | 1.9E-6 | 2.6E-06 | 26 | 654 | 3.5012 | 0.005 | 0.55 |
| 1350 | 1.1E-6 | 9.0E-7 | 1.3E-6 | 27 | 674 | 3.5000 | 0.005 | 0.55 |
| 1360 | 5.8E-7 | 4.7E-7 | 6.6E-7 | 27 | 679 | 3.4987 | 0.005 | 0.55 |
| 1370 | 3.5E-7 | 2.8E-7 | 3.9E-7 | 28 | 684 | 3.4975 | 0.005 | 0.55 |
| 1380 | 2.2E-7 | 1.8E-7 | 2.5E-7 | 34 | 689 | 3.4963 | 0.005 | 0.55 |
| 1390 | 1.3E-7 | 1.1E-7 | 1.5E-7 | 45 | 694 | 3.4951 | 0.005 | 0.55 |
| 1400 | 8.1E-8 | 6.5E-08 | 9.3E-8 | 44 | 704 | 3.4939 | 0.005 | 0.54 |
| 1410 | 4.6E-8 | 3.7E-08 | 5.3E-8 | 46 | 714 | 3.4928 | 0.005 | 0.54 |
| 1420 | 2.9E-8 | 2.3E-08 | 3.3E-8 | 66 | 724 | 3.4917 | 0.005 | 0.54 |
| 1430 | 1.4E-8 | 1.1E-08 | 1.6E-8 | 64 | 735 | 3.4906 | 0.005 | 0.54 |
| 1440 | 8.6E-9 | 6.8E-9 | 9.9E-9 | 76 | 745 | 3.4896 | 0.005 | 0.54 |
| 1450 | 5.8E-9 | 4.6E-09 | 6.6E-9 | 107 | 755 | 3.4885 | 0.005 | 0.54 |

Note. Shown are absorption coefficient (alpha) values at 25°C, 295 K and 300 K, from which the imaginary part of the refractive index can be deduced, plus the real part of the refractive index (n) at 25°C. Also shown are the uncertainty estimates for the tabulated values ($k = 2$) and their normalised temperature coefficient at 25°C. Both temperature coefficients are normalised (e.g., n coefficient = $[1/n]dn/dT$). That for the imaginary part of the index (k) is the same as that for alpha.

^aLess than circa one digit difference in third decimal place between value of n at 25°C and 295 or 300 K over tabulated range. Imaginary part (extinction coefficient, k) calculated as tabulated values of wavelength and alpha multiplied together and divided by 40 000 000 times π (e.g., k at 250 nm at 25°C = $250 \times 1\ 841\ 000 / [40\ 000\ 000 \times \pi] = 3.663$).

The values at 300 K in this range are less than 0.1% higher than those tabulated by Green,² consistent with the uncertainty earlier estimated.² Linear extrapolation using Equation 2 gives the best temperature extrapolation results at these wavelengths although tending to underestimate values at low temperature and to overestimate at high temperatures due to a temperature coefficient that increases with temperature. A more accurate alternative is to use the parametrisation of Frey et al.⁸

At short wavelengths, the dataset of Herzinger et al.¹⁹ has been determined to be the best choice for the absorption coefficient and thereby for the imaginary part of the refractive index. Given this and its remarkable self-consistency as determined by permittivity differentials (Figure 2), it would seem a sensible choice for the real part of the index. This was verified by comparison with other datasets with the results shown in Figure 12. The chosen dataset is in agreement with the results of Jellison,²¹ Humlíček and Šík⁹ and Green² roughly within

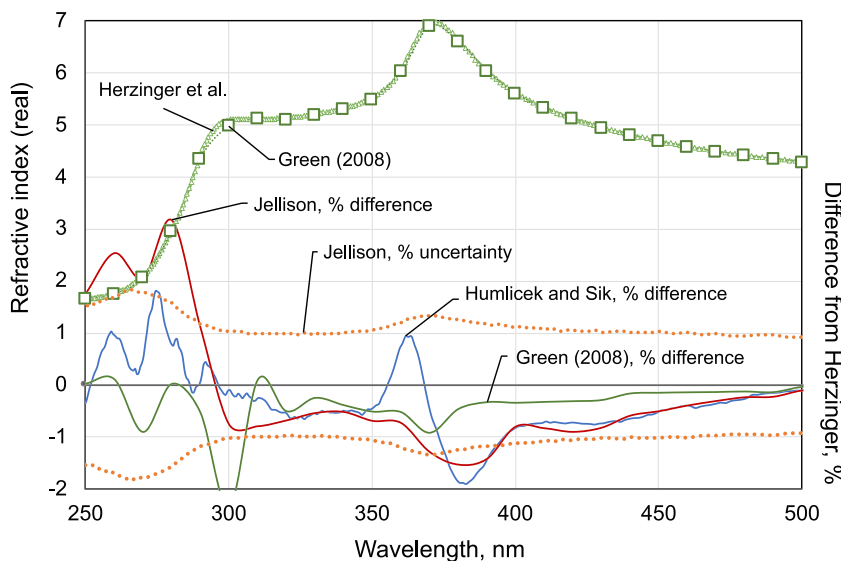


FIGURE 12 Real part of silicon's refractive index over the 250- to 500-nm range showing a comparison between the datasets of Herzinger et al.¹⁹ and Green.² Also shown in the lower part of the figure is the percentage difference between other published datasets and that of Herzinger et al.,¹⁹ as well as the uncertainty estimates ($k = 2$) for the Jellison²¹ dataset that capture most of the observed differences

the uncertainty estimates published by Jellison between 250 and 400 nm. However, agreement improves rapidly beyond 400 nm, reaching better than 0.2% beyond 500 nm.

The dataset of Herzinger et al.¹⁹ extends to 1000 nm, not overlapping with that of Frey et al.⁸, extending from 1100 nm to longer wavelengths. However, at these extremities, the real part of the refractive index in both datasets is circa 0.1% higher than that from Green's earlier tabulation,² indicating excellent self-consistency. Because the changes from Green's earlier dataset² are small and the earlier published temperature coefficients are consistent with those of Frey et al.⁸ over the range of overlap, these earlier coefficients are retained over the 250- to 1100-nm range.

8 | SUMMARY

To correct deficiencies noted in earlier datasets^{1,2} and to take advantage of subsequently published measurement results, refined values of silicon's absorption coefficient and refractive index are tabulated over the 250-nm to 1450-nm range in 10-nm steps at 25°C, together with absorption coefficients at two other common reference temperatures, 295 (nominally room temperature) and 300 K. Temperature coefficients are also tabulated allowing reasonably accurate estimates of optical parameters over the broader –24°C to 200°C range.

Particularly useful in the new compilation was the recent dataset of Schinke et al.,⁶ completely independent of the earlier datasets,^{1,2} useful in determining tabulated values over some ranges as well as in determining final uncertainty estimates. The dataset of Nguyen et al.⁴ was also useful in clearly demonstrating the different absorption coefficient temperature dependencies and appropriate extrapolation approaches in the indirect bandgap absorption region, depending upon whether absorption occurred with phonon absorption or emission. That of Wang et al.²⁶ provided further support for the quality of the earlier data of Weakliem and Redfield¹⁰ and allowed reduction in uncertainty estimates at wavelengths where these were high in the

Schinke et al.⁶ data. Differentiating the dataset of Herzinger et al.¹⁹ showed its superb self-consistency. This together with its good agreement with independent datasets made it the basis for the absorption coefficient tabulation at wavelengths below 430 nm and for the real part of the refractive index at wavelengths below 1000 nm. The more recent and extremely accurate refractive index dataset of Frey et al.⁸ was the clear choice for wavelengths beyond 1100 nm.

Table 1 is provided as an Excel file in the Supporting Information. Also included for convenience is a separate tabulation of the standard AM0, AM1.5G and AM1.5DN reference spectra together with interpolated values of the real and imaginary values of the refractive index and absorption coefficient at the 2002 distinct wavelengths over the 280- to 4000-nm range where these spectra are tabulated (wavelength spacing increasing from 0.5 to 5 nm over the above range).

ACKNOWLEDGEMENTS

The author acknowledges support from the Australian Government through the Australian Renewable Energy Agency (ARENA). The Australian Government does not accept responsibility for any information or advice contained herein. The author also thanks H.A. Weakliem for providing tabulations of his published data and C.M. Herzinger, M. Inokuti, G.E. Jellison Jr., W. Karstens, M. J. Keevers, P. Reece, D.Y. Smith and T. Trupke for providing access to additional data.

DATA AVAILABILITY STATEMENT

The data that supports the findings of this study are available in the supplementary material of this article

ORCID

Martin A. Green  <https://orcid.org/0000-0002-8860-396X>

REFERENCES

- Green MA, Keevers MJ. Optical properties of intrinsic silicon at 300 K. *Progr Photovoltaics*. 1995;3(3):189–192.

2. Green MA. Self-consistent optical parameters of intrinsic silicon at 300 K including temperature coefficients. *Solar Energy Mater Solar Cells.* 2008;92(11):1305-1310.
3. Mitchell B, Juhl MK, Green MA, Trupke T. Full spectrum photoluminescence lifetime analyses on silicon bricks. *IEEE J Photovolt.* 2013;3(3):962-969.
4. Nguyen HT, Rougier FE, Mitchell B, Macdonald D. Temperature dependence of the band-band absorption coefficient in crystalline silicon from photoluminescence. *J Appl Phys.* 2014;115(4):043710.
5. Schinke C, Bothe K, Peest PC, Schmidt J, Brendel R. Uncertainty of the coefficient of band-to-band absorption of crystalline silicon at near infrared wavelengths. *Appl Phys Lett.* 2014;104(8):081915. <https://doi.org/10.1063/1.4866916>
6. Schinke C, Peest PC, Schmidt J, et al. Uncertainty analysis for the coefficient of band-to-band absorption of crystalline silicon. *AIP Advances.* 2015;5:067168. <https://doi.org/10.1063/1.4923379>
7. Daub E, Wuerfel P. Ultralow values of the absorption-coefficient of Si obtained from luminescence. *Phys Rev Lett.* 1995;74(6):1020-1023.
8. Frey BJ, Leviton DB, Madison TJ. Temperature dependent refractive index of silicon and germanium. *Optomech Technol Astron.* 6273. <https://doi.org/10.1117/12.672850>
9. Humlíček J, Šík J. Optical functions of silicon from reflectance and ellipsometry on silicon-on-insulator and homoepitaxial samples. *J Appl Phys.* 2015;118:195706. <https://doi.org/10.1063/1.4936126>
10. Weakliem HA, Redfield D. Temperature dependence of the optical properties of silicon. *J Appl Phys.* 1979;50(3):1491-1493.
11. Jellison GE, Modine FA. Optical functions of silicon at elevated temperatures. *J Appl Phys.* 1994;78(6):3758-3761.
12. Vuye G, Fisson S, Van VN, Wang Y, Rivory J, Abeles F. Temperature dependence of the dielectric function of silicon using in situ spectroscopic ellipsometry. *Thin Solid Films.* 1993;233(1-2):166-170.
13. Schenk A. Finite-temperature full random-phase approximation model of band gap narrowing for silicon device simulation. *J Appl Phys.* 1998;84(7):3684-3695. <https://doi.org/10.1063/1.368545>
14. Altermatt PP, Schenk A, Geelhaar F, Heiser G. Reassessment of the intrinsic carrier density in crystalline silicon in view of band-gap narrowing. *J Appl Phys.* 2003;93(3):1598-1604.
15. Sproul AB, Green MA. Improved value for the silicon intrinsic carrier concentration from 275 to 375K. *J Appl Phys.* 1991;70(2):846-854.
16. MacFarlane GG, McLean TP, Quarrington JE, Roberts V. Fine structure in the absorption-edge spectrum of Si. *Phys Rev.* 1958;111(5):1245-1254.
17. Lautenschlager P, Garriga M, Vina L, Cardona M. Temperature dependence of the dielectric function and interband critical points in silicon. *Physical Review B.* 1983;36(9):4821-4830.
18. Yu P, Cardona M. *Fundamentals of Semiconductors: Physics and Materials Properties.* 4thed. Berlin, Heidelberg: Springer; 2010 10. 1007/978-3-642-00710-1.
19. Herzinger CM, Johs B, McGahan WA, Woollam JA. Ellipsometric determination of optical constants for silicon and thermally grown silicon dioxide via a multi-sample, multi-wavelength, multi-angle investigation. *J Appl Phys.* 1998;83(6):3323-3336.
20. Aspnes DE, Studna AA. Dielectric functions and optical parameters of Si, Ge, GaP, GaAs, GaSb, InP, InAs, and InSb from 1.5-6.0 eV. *Phys Rev B.* 1983;27:985-1009.
21. Jellison GE. Optical functions of silicon determined by two-channel polarization modulation ellipsometry. *Opt Mater.* 1992;1(1):41-47.
22. Tao K, Lai T, Zhang Y, Yu Z, Mo D. The temperature dependence of the interband critical points in silicon within a fractional-dimensional space approach. *J Phys Condens Matter.* 2004;16(18):3041-3051.
23. Lefebvre P, Christol P, Mathieu H. Confined excitons in semiconductors: correlation between binding energy and spectral absorption shape. *Physical Review B.* 1995;52(8):5756-5759.
24. Dash WC, Newman R. Intrinsic optical absorption in single-crystal Germanium and Silicon at 77°K and 300°K. *Phys Rev.* 1955;99(4):1151-1155.
25. Geist J. Silicon revisited. In: Palik ED, ed. *Handbook of Optical Constants of Solids III.* New York: Academic Press; 1998:519-529.
26. Wang H, Liu X, Zhang ZM. Absorption coefficients of crystalline silicon at wavelengths from 500 nm to 1000 nm. *Int J Thermophys.* 2013;34(2):213-225. <https://doi.org/10.1007/s10765-013-1414-2>
27. Anagnostopoulos C, Sadasiv G. Fine structure in the optical-absorption edge of silicon. *Phys Rev.* 1973;7(2):733-739.
28. Keevers MJ, Green MA. Extended infrared response of silicon solar cells and the impurity photovoltaic effect. *Solar Energy Mater Solar Cells.* 1996;41/42:195-204.
29. Svantesson KG, Nilsson NG. Determination of the temperature dependence of the free carrier and interband absorption in silicon at 1.06mm. *J Phys C: Solid State Phys.* 1979;12(18):3837-3842.

SUPPORTING INFORMATION

Additional supporting information may be found in the online version of the article at the publisher's website.

How to cite this article: Green MA. Improved silicon optical parameters at 25°C, 295 K and 300 K including temperature coefficients. *Prog Photovolt Res Appl.* 2022;30(2):164-179.
doi:10.1002/pip.3474